IOSR Journal Of Applied Physics (IOSR-JAP)
e-ISSN: 2278-4861.Volume 14, Issue 5 Ser. I (Sep. – Oct. 2022), PP 52-65
www.Iosrjournals.Org

Structure-Property Correlation in Lead Borate Glass with Fixed Ratio of Samarium Oxide

Heba M. Ali[a,*], M. M. Nassery[a], k. Salaheldin [a] Mohammed Ezzeldien[a,b]
[a]*Physics Department, Faculty of science, South Valley University, 83523, Qena, Egypt.*
[a,b] *common First Year Deanship, Jouf University, P.O. Box:2014, Sakaka, Saudi Arabia*
**Corresponding authors: E-mail addresses:hhebaali.201664@gmail.com(Heba. M. A)*

Abstract
To adopt the correlation of structural and property,a novel series of borate glass system has a stochiometric composition of [(78 – x) B_2O_3 – x PbO – 20 Na_2O – 2 Sm_2O_3] where x = 0, 5, 10, 15 and 20 mol.%was successfully synthesized by Melt-Quenching method. The samples were scrutinized by a set of techniques such as XRD, density, FTIR, DSC, and UV-visible measurements. The density was measured to shed light on macrostructural of the samples. FTIR spectra proved the existence of BO_4 to BO_3 conversion. FTIR spectra answered about a longstanding important question is the role of PbO at low loadings. Actually, at (x = 0 – 20), the boron coordination was converted from 3 to 4, and lead behaves as a modifier with positive charge 2.The DSC measurement was monitored to extract the thermal features of the samples. The absorption spectra exhibit sixteen absorption bands related to Sm^{3+}ions, among them, four transitions [$^6H_{5/2} \rightarrow {}^6F_{11/2}$, $^6F_{9/2}$, $^6F_{7/2}$, and $^6F_{5/2}$ corresponding to 1075, 1223, 1366, and 1470 nm] have relatively higher intensities. Such intensive peaks are promising for using in orange-red lightening emitting and photonics devices. Undergoing of the absorption edges to shift towards the high wavelength reflects a deterioration in the optical band gap energy. The enhanced Urbach energy were precisely evaluated driven by the lead oxide addition. Other related optical parameters were obtained and then discussed. The nonlinearity analysis was confirmed the applicability of such samples for optoelectronic applications. The present PbO-doped borate glasses suggest a distinct structural/properties interaction make them suitable for optoelectronic and optical devices.

Keywords:*Sm^{3+} and Pb^{2+} ions, borate glass, nonlinearity analysis, thermal stability, optoelectronic applications.*

Date of Submission: 18-09-2022 Date of Acceptance: 03-10-2022

I. Introduction

Recently, glass material is a perfect and very effective for using in the optical and the optoelectronic applications. Because it has appealing physical properties like mechanical and thermal stability, high optical transparency, and chemical resistance [1,2,3,4].Inorganic glasses doped with rare earth elements are important materials. They have subtle properties such as high thermal stability, great flexibility, high light yield, and high density [5]. These motivating properties make them a decent contender utilized in the optics realm [6,7] such as optical amplifier, solid state lasers, color displays, optical sensors [8], white light emitting diodes (WLEDS) [9], infrared laser windows, scintillation materials, and Memories [10]. The released strong emission of *4f-4f* transitions from trivalent rare earth ions makes them have distinct applications. However, the main outface is to choose the right rare earth ion for enhancing the optical properties. Among series of lanthanides ions, samarium is one of many modifying ions that exhibits two valance states, namely $Sm^{2+}$and Sm^{3+}. Samarium ions have considerable optical properties make them have significant importance in technological applications [11, 12]. Specifically, trivalent samarium ions (Sm^{3+}) are suitable modifiers for improving optical performances because of they have high quantum efficiency, small phonon energy (~700cm^{-1}) and great corrosion resistance[13,14]. Consequently, the amalgamation of such ions in glass material renders them suitable candidates for many applications like fluorescent display devices, visible lasers, hole burning, energy generation, biomedical, telecommunication, and orange color emitting [6,15,16].

Heavy metal oxides (HMO) are attractive ions that characterize with a high density, high refractive index, easy to form, high stability and polarizability, and high infrared transparency [17]. The glasses mixed with HMO (here, PbO) exhibit a high transparence, good structural, thermal characteristic and easy to prepare, making such glasses have high applicability in optoelectronics and as photoconductive materials [18]. Among heavy metal oxides, lead oxide exhibits a high linear and non-linear refractive index, large energy gap, large

atomic number, good polarizability. In addition to it enhances the glass's density and stability and low durability. These motivating properties open the way towards lead oxide to act as modifier or former,depending on their competence to formbonds with both covalent and ionic naturebetween lead and oxygen in the glass network[5, 19, 22]. Glass materials mixed with lead oxide have decent contribution in many applications like thermoelectric devices [17], protection from harmful radiation, photonic and optoelectronic, laser hosts, and as a shielding material against gamma ray[17,19]. On the other hand, the solids containing Pb^{2+} ions are toxic for the environment, so the high concentration of PbO involved here is 20 mol. %, which is expected to be ecofriendly. Also, they must be carefully treated[18, 23].

Borate glass is one of the base materials that have a wide range of doping with various ions and are considering good choice to produce appealing hosts for distinct applications such as solid laser hosts, thermal sensors, ultraviolet optics, and optical devices [24]. Such distinct applications of borate are reflecting from being have special physical characteristics like low meting point, great thermal stability needed for working devices, flexibility, easy to manufacture, high ultraviolet transparency, in addition to they have high ability to form two structural units [22,25,26]. Addition of alkali oxides like (Na_2O,Li_2O, ….., etc) leads to improve and enhance the physical features of borate glass such as lowering the phonon energy, increasing the homogenization, andmitigating the melting point [27].

In light of the aforementioned properties and applications, investigating the PbO/B_2O_3 structural interaction is an objective key in comprehending the features of such lead borate glasses.

Here, for the sake of tailoring the structural, thermal, and optical features of borate glass composition with fixed ratio of samarium oxide (i.e., 2 mol. %) and doped with different concentrations of lead oxide. Melt quenching method was exploited to prepare the samples. Some distinct findings were, here, obtained and will be discussedbelow. Thefindings of this studyguide the researchers to open theirideas into the optoelectronic realm.

II. Experimental Procedures

2.1. Samples Fabrication

Thequenching of molten was here applied, as a method, to prepare a novel quaternary model of borate glass system has a nominal composition of [(78 – x) B_2O_3 – x PbO – 20 Na_2O – 2 Sm_2O_3] where the lead oxide was intercalated into the system as follows: [0, 5, 10, 15 and 20] mol. %. High purity chemicals of H_3BO_3, Na_2CO_3, Sm_2O_3 and PbO were used as they were purchased. These raw chemicals were carefully chosento support the small batch-free time of molten, and weighting in quantities (in mols. %) and were carefullyground in agate mortar. The resulting fine particles rapids the liquefaction process. The mixing powder put into a porcelain crucible, 50 ml. The mixture was melted in a digitalized electrical oven at 1100 ˚Cfor 45 minutes. The melted mixture was carefully stirred to ensure high degree of the homogeneity. After, the molten was poured and rapidly quenched between two circular stainless-steel plates at 28˚C.Glassy samples, which have a disk shape, were obtained.The samples exhibit transparency, homogeneity, and bubbles and cracks-free.Then they were stored in a desiccator to prevent damages from surrounding environment.

2.2. Samples Characterization

X-ray diffraction was applied to the samples (powder) to emphasize the structural nature of the glass samples by using diffractometer type of Bruker D8 advance. The wavelength ofX – ray source is 1.541 Å. Data were obtained from 20° to 90°. The operating power of X – ray tube is 1200 Watt.Density measurement of the glass samples were measured via Archimedes' principle by using Toluene with density (0.867 g/cm^3), as a submerged fluid. The obtained values of density were measured using a digital electronic balance (Setra BL-410SLCD) with accuracy ± 0.001 g. To guarantee a minimal error and precise values,five trails for each sample, in the same conditions, were conducted to obtain the values of density. Moreover, the related parameters of such glass samples were calculated via the measured density. FT-IR spectra of glass samples were measured in the wavenumber starts from400$cm^{-1}$to 4000 cm^{-1} using FT-IR Nicolet 6700 spectrometer. In FT-IR measurements, high purity KBr and powder samples were mixed then pressed into small disks by a compressor.The DSC measurement was conducted for all samples using the "Discovery SDT 650-Simultaneous DSC-TGA/DTA, USA" instrument. The wight of powderwas in order of 8 mg. This experiment was proceeded under N_2 atmospherewith a constant heating rate 20 ℃/min over a temperature range from room temperature to 1000 ℃. Finally, the optical absorption spectra of the samples were collected in wavelength range 200 - 2500 nm, using (JASCO V-670) spectrophotometer. A standard normalization processes are applied to spectra of FT-IR and optical absorption employed to eliminate the variation in all samples. In addition, the estimated errors ofmeasured values were calculatedand recorded in tables.

III. Results and Discussion

3.1. X-Ray Diffraction

XRD analysis was utilized to confirm the proper preparation of all samples. Fig. 1 displays the XRD spectra of selected samples (i.e., 0 mol. %, and 20 mol. %). The figure exhibits no sharp peaks detected in the spectra, confirming the amorphous entity of the samples.

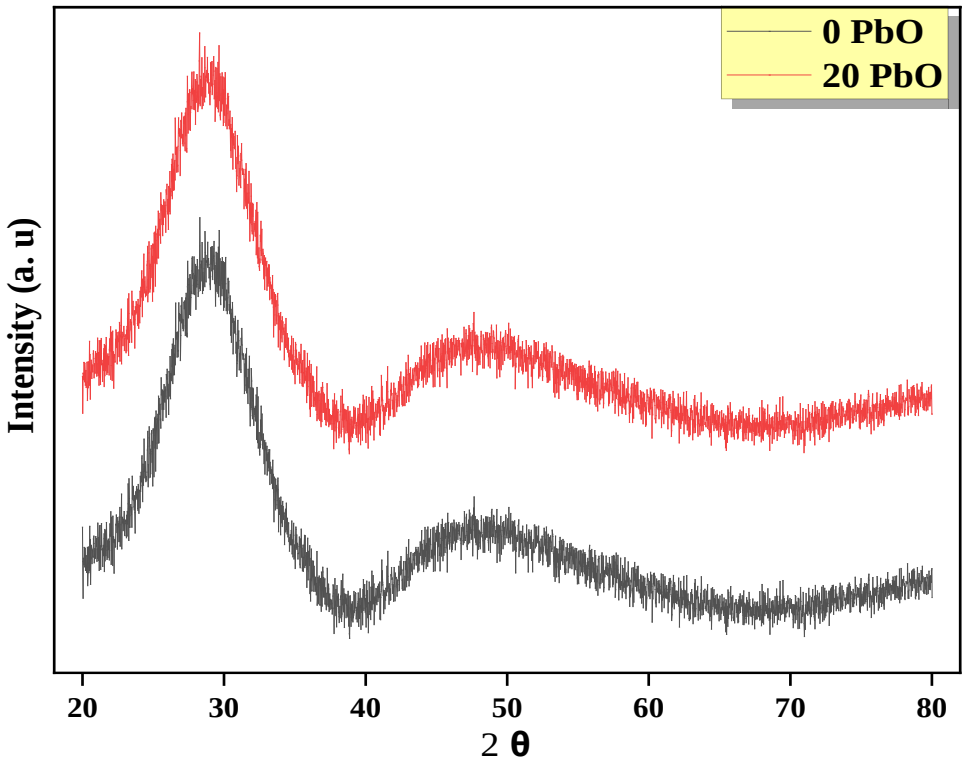

Fig. 1: XRD diffractograms of the selected prepared samples (10 and 20 mol. %).

3.2. Density Measurement

It is important to explicitly understand the structural changes in the glass matrix, therefore studying the measured density (ρ) and the calculated molar volume (V_m) in conjunction with the other related parameters like ionic radius (R_i), number density of Pb (N), $d_{B\text{-}B}$, Pb molar concentration and refractive index (n) for all samples. The values of these factors were tabulated in Table 1. In addition to these parameters were calculated according to Ref. [28]. The variation between the measured density (ρ) and the average boron-boron separation ($d_{B\text{-}B}$) with the PbO content was shown in Fig. 2. It is cleared that the density increases gradually from (2.40 g/cm^3) for the Pb-free sample to (3.16 g/cm^3) for highest Pb concentration, (i.e., increased by 32%). This is likely related to the insertion of higher molecular weight (223.2) g/mol and higher density (9.53 g/cm^3) of PbO at the expense of lighter molecular weight (69.63) g/mol and lower density (2.46 g/cm^3) of B_2O_3. Additionally, the substitution of B_2O_3 by PbO creates alterations to the boron-oxygen assembly, and easy to create more of BO_4 structural units (as shown next in FTIR section). For the sake of confirming of the induced structural compactness, the $d_{B\text{-}B}$ was found to decrease with PbO addition, as shown in Fig. 1, supporting the dense compactness of the glass network.

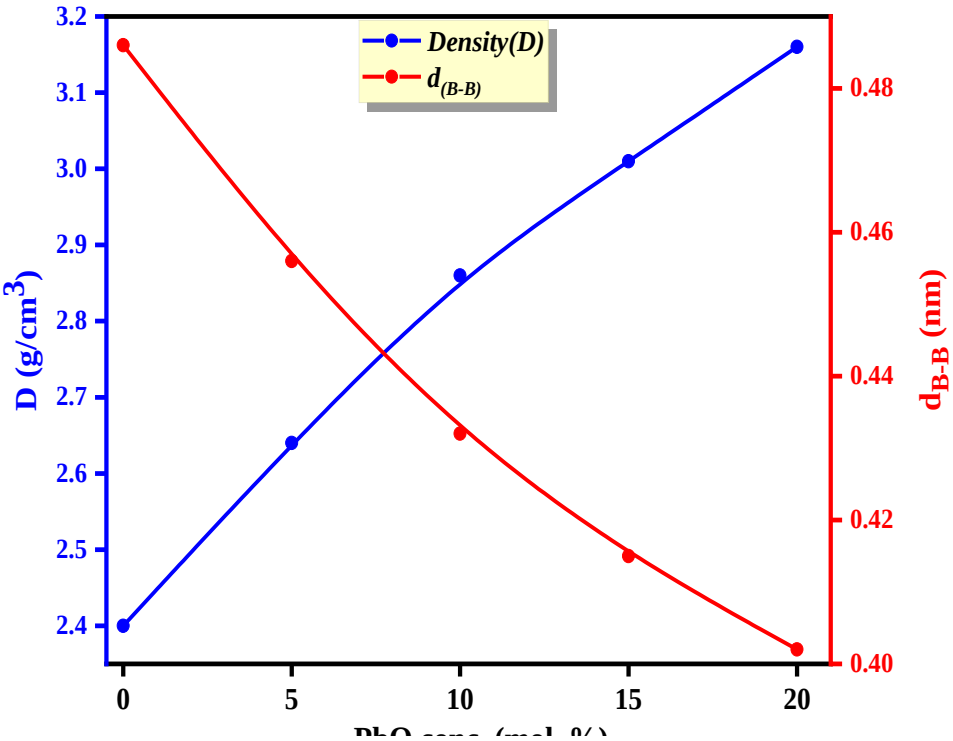

Fig. 2: The measured density, *D*, and average boron-boron separation, d_{B-B} against PbOadditives.

On the other hand, the molar volume, V_m, of the prepared glass samples was noticed to increase from 30.46 cm^3/mol for Pb-free sample to 32.97 cm^3/mol for highest Pb concentration here doped with PbO content, (i.e., enhanced to 9%). This increase in V_m is attributed to more possibilities such as the largest ionic radius of Pb^{2+} ion (2.02 Å) compared to that ofB^{3+}ion (0.2 Å)[1,18,29]. Another possibility represents in the doping by higher molecular volume of PbO (23.42 g/mol) compared toB_2O_3(28.3 g/mol), leading to stretching of the network. Additionally, number density ofPb^{2+} ions, *N*,(i.e., Pb^{2+} ions concentration) was found to augment due to PbO pumping through the glass matrix. Factually, the molar concentration is normalized with the PbO concentration. The molar concentration was normalizedto fixed value $(1.895\pm0.0035)\times10^{20}(1/1cm^3.\,mol.\,\%)$. This fixed value confirms the proper stoichiometry of the prepared glass samples.

PbO conc. (mol. %)	ρ (g/cm^3) ±0.010	V_m (×cm^3/mol) ±0.0298	*Ri* (nm) ±0.0001	*N* (10^{21}/cm^3) ±0.0098	Pb^{2+} Molar concentration (10^{19}/cm^3.mol.%) ±0.0035	d_{B-B} (nm) ± 0.000142	N_4 (%)	NBO (%)
0 Pb	2.40	30.46	0	0	0	0.486	46.09	28.74
5 Pb	2.64	30.83	1.008	0.97	1.95	0.456	49.91	32.99
10 Pb	2.86	31.27	0.803	1.92	1.92	0.432	51.30	31.49
15 Pb	3.01	32.04	0.708	2.81	1.87	0.415	52.84	28.03
20 Pb	3.16	32.97	0.649	3.65	1.82	0.402	52.92	26.89

Table 1: Density, molar volume, interionic distance, Pb^{2+} ions concentration (*N*), Pb molar concentration, the average boron-boron separation, N_4 ratio and NBO ratio for all glass samples.

3.3. FTIR Analysis

FTIR is a basic tool to emphasizes the alteration of structure in the samples and understand the nature of several vibration modes of the atoms and their absorption peaks. Fig. 3 manifests the FTIR spectra for the prepared samples. The FTIR spectra of borate glasses can be observed through three regions with wavenumber from 400 cm^{-1} to 1600 cm^{-1} as follows [30]:

- The bending vibrations are between 600-800 cm^{-1}, belong to BO_3 units.
- BO_4 groups are enveloped between 800-1200 cm^{-1}.
- Finally, the stretching vibrations located from 1200 to 1600cm^{-1}, belong again to BO_3units.

The measured spectra ofsamples exhibit a set of characteristic bands that are furnished from 400 cm^{-1} to 1600 cm^{-1}. For more specific assignments of these structural bands, a deconvolution process was exploited for a deep understanding of the structural changes in the glass system. The deconvolution process was performed by utilizing a set of Gaussian functions software.

Based on the bands resulting from the deconvolution process, a weak band, is attributed to vibration of sodium's cation, was observed to tail near 410 cm^{-1}[30,31], while another characteristic band is pinned at 475cm^{-1}, which attributed to the vibration of lead's cation [32]. This band was observed to enhance in its intensity due to the loading of lead oxide to the network.In addition to a vibrational band was observed at 520cm^{-1} due to the B-O-B bending vibrations resulting fromdeformations of boroxol ring angles [30,33]. The existence of asymmetric (symmetric) bending vibrations of octahedral BO_3 functional groups was found to be located at 626 (698 cm^{-1}) [30,33,34].

On the other hand, the absorption bands are located in the BO_4spectral region at 852, 945 and 1054 cm^{-1} are attributed to the BO_4stretching vibrations[30, 34, 35]. Specifically, the characteristic band at 852 cm^{-1}(symbolized by *) is essentially assigned to B-O stretching vibration of non-bridge oxygen (NBOs) in BO_4 group [30,35]. The used decomposition method suggested that the intensity of this band undergoes a spectral mitigation with increasing of the PbO contents, which in its turn leads to mitigate the overall NBO ratio in the glass matrix. This decrement is due to the replacement of PbO with high atomic radius at the expense of the $B_2O_3$with low atomic radius [29,36]. This variation helps to createmore ofBO_4 structural groups, in a good accordance with the increasing in density.

In the last region, at the high wavenumber, a set of three peaks were pinned at 1236, 1326 and 1406 cm^{-1} that are again ascribed to stretching vibrations of BO_3 functional group. Especially, the first peak (i.e., 1236cm^{-1}) (marked by #) is pertained to the B-O stretching vibrations of non-bridging oxygen's of trigonal units, $(NBOs)_{BO_3}$[34]. This band was observed, along all samples, to undergo some spectral modifications such as intensity decrement and areal narrowing with the addition of PbO contents. Using the total areal under peak, NBO ratios can be obtained by the equation*Morshidy et. al*[30]: $NBO = NBO^{*}_{BO_4} + NBO^{\#}_{BO_3}$.Table 1 shows the values of NBO ratios, which indicate a prominent deterioration in NBO concentration. More informative modifications can be inferred by N_4 parameter. To know the fraction of tetrahedral BO_4 unitsto the total number of structural borate groups, N_4 parameter can be obtained exploiting the total area under peaks resulting from the Gaussian deconvolution method as[28, 30]: $N_4 = BO_4/(BO_3 + BO_4)$. The values ofN_4 are listed in Table 1. The values ofN_4ratios were gradually increased with the increasing in the concentration of PbO. The increment ofN_4, supported by deterioration in NBO, suggested a conversion from BO_3 to BO_4 groups, proving an open structure of glass network, in a decent agreement with density measurement.

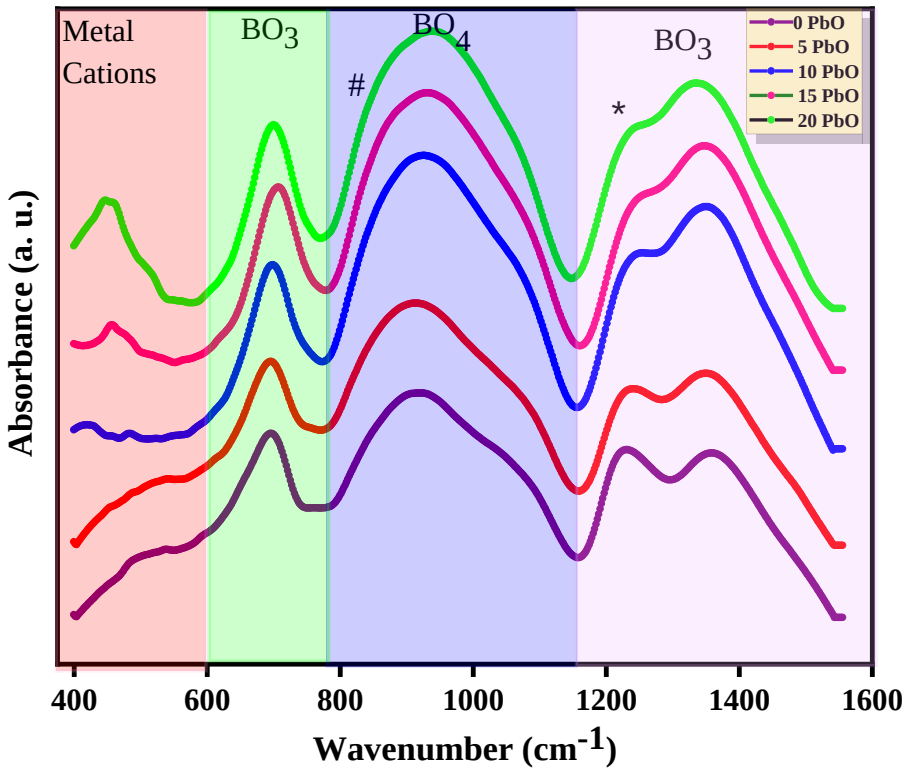

Fig. 3: Vibrational infrared spectra of all proposed samples.

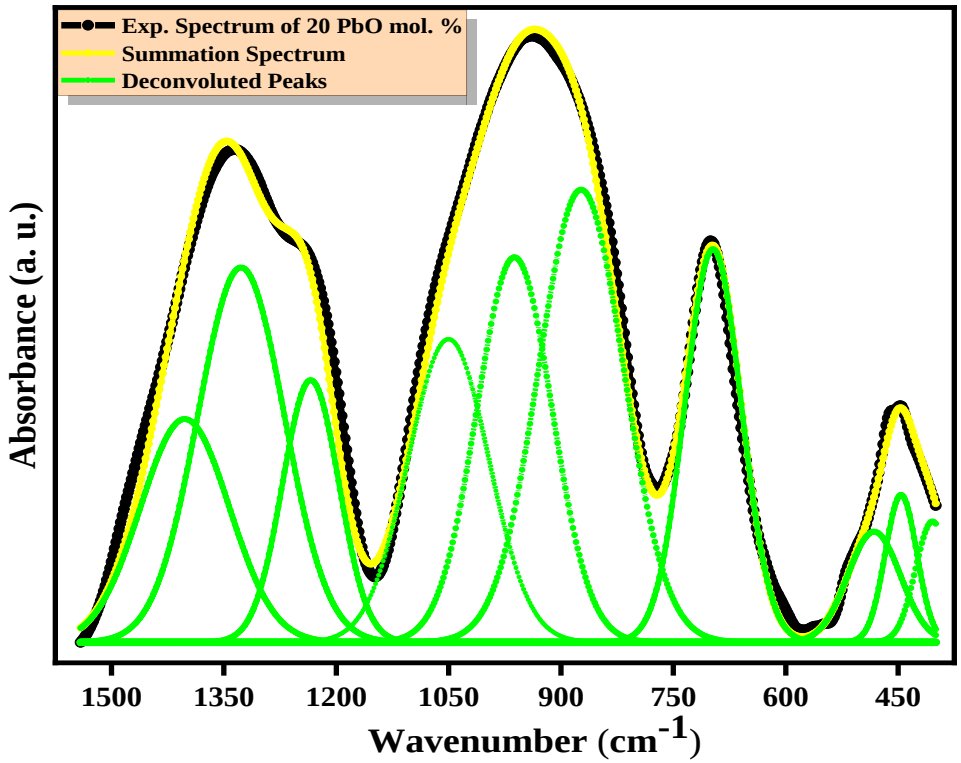

Fig. 4: A pictorial description for the simulated spectrum through a deconvolution process of the concentration 20 mol. % of PbO.

3.4.Differential Scanning Calorimetry (DSC)

Thermal parameters, such as glass transition temperature, crystallization temperature, melting temperature, and glass stability, are more important informative parameters for getting a thermal properties of glass materials. The samples were measured at a fixed heating rate 20 ℃/min, in the range of 100 ℃ up to 900

℃. The samples exhibit significant thermal features as characteristic endothermal peaks followed by significant exothermal peak.The glass transformation temperature, crystallization temperature, melting temperature, and glass stability were calculated and furnished in Table 2. These parameters exhibit an increment with the addition of PbO content. The augmentation in the transforming temperature from 424 ℃ to 485℃, Fig. 5, and the crystallization temperature may be attributed to more factors, which explained based on the addition ofPbO, such as there is a modification in the bond nature of network cations (i.e., an increment in the ionic bonds of Pb-O compared to B-O). Besides, the augmentation in the cross-linking density between the atoms of system here involved [37].

Thermal stability, (T_c -T_g), is a potent informative parameter measures a temperature range within it the glass does not crystallize. It is well-known that the higher glass stability exhibits a lower tendency to the crystallization. Therefore, it is a better glass quality. During working of the optical devices such as optical fiber and optoelectronic devices, they undergo repeated and prolonged heating cycles. Such these thermal cycling leads to creation of micro-crystals that act as scattering centers, attenuating the light. Generally, the thermal stability should be more than or equal 100 ℃ to prevent such these micro-crystals [20,37,38].

Here, the obtained values of thermal stability tend to be at about average value of 135℃, Fig. 5. The augmentation in thermal stability values may be back to the addition of Pb^{2+} ions which strains the glass network and delays the crystallization process. Other important factor is the hike in the molar volume, as referred in density measurements. Such value renders the glass samples are very applicable in optical devices.
Another salient parameter, which is called "Hruby's parameter, (H_R)" is also appointing to determine the thermal stability of prepared glasses from DSC thermograms. It is determined from the relation [38,40,41]:

$$H_R = \frac{T_c - T_g}{T_m - T_c} \quad (1)$$

It is well-known that [38, 39], the thermal stability extracted from Hruby's relation should be greater than 0.1 for more thermally stable glasses. The average value of Hruby's parameter is about 0.77, verifying a thermally stable glass samples, and thus they are more suitable for optoelectronic applications.

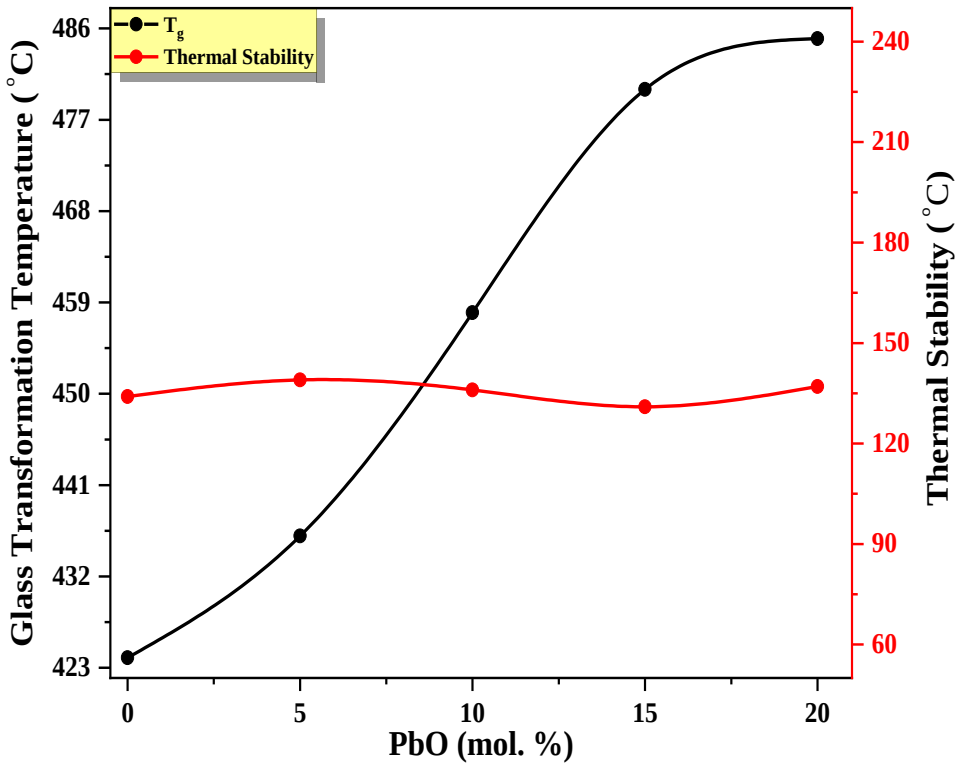

Fig. 5: Glass Transformation temperature and thermal stability against the concentration of PbO for all proposed samples.

Sample (mol. %)	T_g (℃)	T_C (℃)	T_m (℃)	(T_c -T_g) (℃)	H_R
0 Pb	424	558	736	134	0.75
5 Pb	436	575	748	139	0.80
10 Pb	458	594	760	136	0.81
15 Pb	480	611	788	131	0.74
20 Pb	485	622	808	137	0.73

Table 2: DSC parameters of all prepared glass samples.

3.5. Optical Characterization

The following sections deal with the optical characteristics of the prepared glass system. The study of the optical mechanism of materials (e.g., glass) proved to be powerful key information for comprehending the behavior of light propagation through the materials.

3.5.1 Absorption Spectra

The optical absorption measurements are essential key to understand the electronic band structure, the nature of bonds, and the optical transitions in the glass material. Fig. 6 (a-b) displays the UV-VIS-NIR absorption spectra for the studied glass system. Generally, the optical absorption spectra can be divided into four major regions as indicates in Fig. 6 (a-b). As shown, the first region is the saturation region, then the second region is related to the absorption glass edge, in which the electrons can absorb an energy is sufficient to move them from the valence to conduction band, reflecting the energy band gap (E_g) of material. The distinctive tail region of the glass spectra (i.e., Urbach tail) is mainly correlated to the disorder in the materials (i.e., the created localized states), providing the Urbach energy (E_u). Then along with the higher wavelengths, the absorption spectra exhibit characteristic bands formed by the electronic transitions.

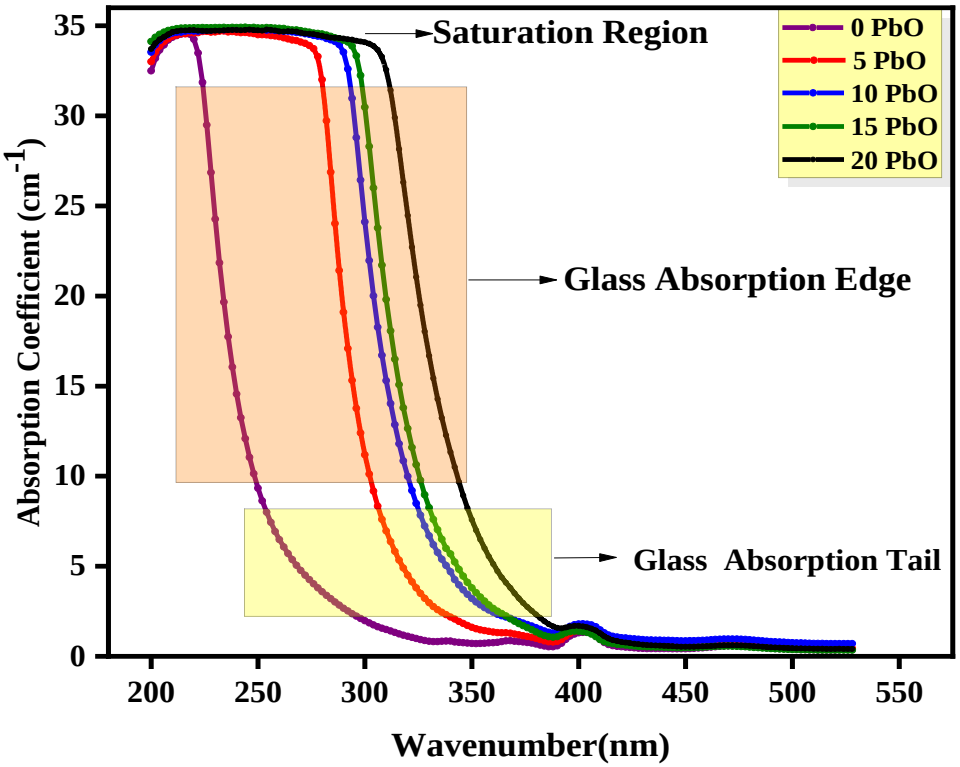

Fig. 6 (a-b): Spectral regions of saturation domain, glass absorption edge and absorption tail for all samples.

Here, samarium oxide was utilized as a modifier oxide to enhance the optical properties of materials. Sm^{3+}ions exhibit a set of characteristic absorption bands formed by the *4f*-*4f* electronic transitions. These transitions are

highly affected the host matrix of material and dopant content[11-14]. Such transitions revealed distinct Sm^{3+} *4f*-4*f* electronic transitions, which are assigned as the transitions from the Sm^{3+} ground state ($^6H_{5/2}$) to the higher energy levels [42]. There are sixteen absorption bands seen in the optical absorption spectra of Sm^{3+}ions, which are in the wavelength range (300-1800 nm), are attributed to the following transitions: $^6H_{5/2} \rightarrow$ [$^6H_{9/2}$, $^4D_{3/2}$, $^6P_{7/2}$, $^4L_{15/2}$, $^6P_{3/2}$, $^6P_{5/2}$, $^4G_{9/2}$, $^4I_{13/2}$, $^4M_{15/2}$, + $^4I_{11/2}$, $^6F_{11/2}$, $^6F_{9/2}$, $^6F_{7/2}$, $^6F_{5/2}$, $^6F_{3/2}$, $^6H_{15/2}$]at 343, 360, 374, 388, 402, 416, 438, 460, 476, 943, 1075, 1223, 1366, 1470, and 1521 nm, respectively. These transitions have been assigned based on the data from Refs[12,43,44]. Among these transitions, there are four transitions [$^6H_{5/2} \rightarrow$ $^6F_{11/2}$, $^6F_{9/2}$, $^6F_{7/2}$, and $^6F_{5/2}$ corresponding to 1075,1223, 1366, and 1470 nm] have relatively higher intensities. Thus, they are attractive transitions for orange-red lightening emitting devices, white LEDs, and solid lasers [7, 12, 43, and 44].

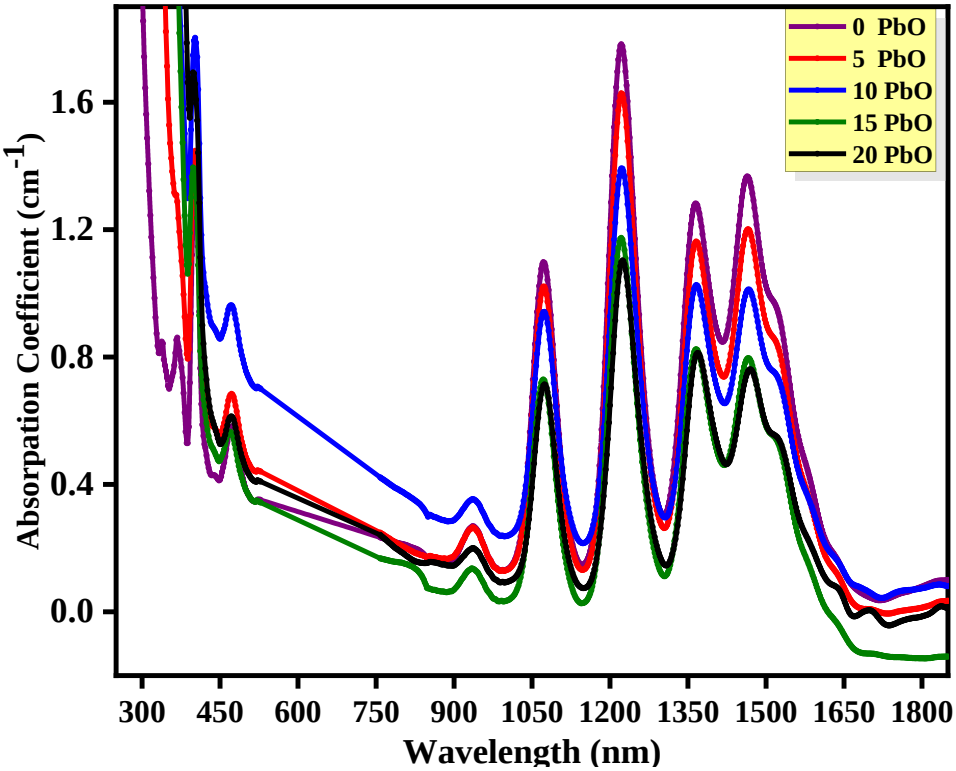

Fig. 6 (a-b): Normalized optical absorption spectra scaled up against PbO concentration for all glass samples.

3.5.2 Band Gap Energy

Band gap Energy (E_g) is considered as an important tool to determine the required energy of electrons to across the valance band reaching to conduction band. It could be determined from Davis and Mott relation [45]:

$(\alpha h\nu)^n = A(h\nu - E_g)^n$ (2)

Where is α the absorption coefficient, hν is the energy of incident radiation, E_g is the band gap energy, A is a constant, and n is an index relies on type of transitions and material nature. For direct allowed, indirect allowed, direct forbidden, and indirect forbidden transitions, n is (1/2, 2, 1/3, and 3) [19,30].In the amorphous materials, such as glass, the best fit of equation x is obtained when n = 2 for indirect allowed transition. Tauc's plot was exploited for representing equation 2 to extract the optical band gap energy. The inset part of Fig. 7 exemplifies Tauc's plot of sample 10 PbO, all samples' spectra were undergone the same routine. The determination of optical gap energy was brought from the protraction of linear portions of Tauc's plot. Fig. 7shows the energy band gap values for all prepared samples. The values of band gap energy were observed to mitigate with PbO content. Initially, to understand such deterioration in the gap energy, the glass absorption edge should be studied for all samples. It is observed that the glass edges were found to shift towards the high wavelength (i.e., towards the low energy), consequently one can say that the glass edges of all samples undergo a red shift, as shown in Fig. 6 (a). The origin in such shifts back to mainly factors that related to the dopant ions (PbO). The shrinking in the bond strength, where the bond strength of B-O is higher than the bond strength of Pb-O. Additionally, the PbO doping can deform the network, causing a supplementation of the oxygen cloudby

the creation of lead's structural units, such factor may be induced more looser electron into the glass system, causing an increment of the electronic conduction, therefore the band gap is mitigated [1,19,35,46].
Urbach energy is one of the essential characteristic parameters to measure the disorder inthe glass samples**.** The absorption tails, shown in Fig. 6, of the glass samples are exploiting to describe Urbach energy. The clear broadening of such part confirms the amorphous nature of the samples, as proved in XRD measurements. The absorption tails can be exploited to determine Urbach energy using the following Urbach relation [47]:

$$\text{Ln}(\alpha) = \text{Ln}(\alpha_0) + \frac{h\upsilon}{E_u} \quad (3)$$

whereα_0 is a constant, and E_u is Urbach energy. The values of Urbach energy can be obtained by plotting the relation between the Ln (α), as Y-ordinate, and photon energyas X-ordinate. The inverse of the slopes of the linear portions in the curves provide the values of Urbach energy. The obtained values are drawn to naked eyes in Fig. 8. The clear augmentation in Urbach's values with PbO additives, may be due to the internal structural fluctuations causing more defects in the forbidden band gap, increasing the disorder in glass samples [1, 35].

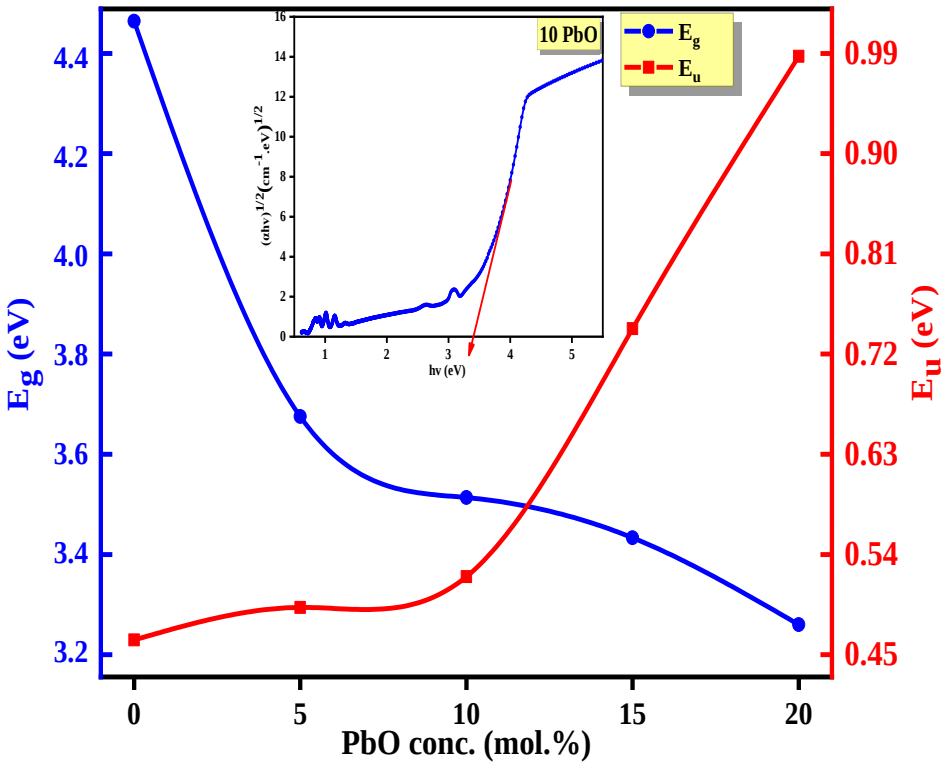

Fig. 8: Optical gap energy and Urbach energy against PbO concentration. The inset part shows the reliance of $\sqrt{\alpha h\upsilon}$ on the energy of photon (hυ) for all raw spectra. The red line presents the straight section from which the gap energy estimated.

3.5.3 Optical Parameters

In this section, other optical parameters are related, too, through the band gap and Urbach energy. To investigate the behavior of material being it behaves as insulator or metal, the metallization criterion, *M*, can be exploited to do this job. When metallization criterion is closed to "1", the glass samples behave as insulators, while when they behave as metals, metallization criterion nears "zero". The metallization criterion can be calculated, relying on band gap energy values, from the next equation [33]:

$$M^2 = \frac{E_g}{20} \quad (4)$$

where the E_g is the energy band gap. Table 3 illustrates the obtained values of *M*. The observed enhancement of the metallic behavior is clear in its criterion's values that changes from 0.47 to 0.44 eV. This decrement in the values of *M* is due to the nearby of valenceband to conduction band, lowering the energy gap. Steepness parameter is a mirrored coefficient to Urbach energy. It is used to describe the broad of the tail of the localized states in the band gap. Steepness coefficient, *S*, can be related to Urbach energy through the following g relation [1,35]:

$$S = \frac{K_B T}{E_u} \quad (5)$$

where$K_B$is the Boltzmann constant, *T* is the room temperature in kelvin, andE_U is the Urbach energy. Table 3 shows the calculated values of steepness coefficient. It is observed that the values of *S* deteriorate with the PbO addendum. Such deterioration reflects an increment in the tails broadening of samples (i.e., increment the band tail width). This is due to the improved localized states in the band gap (i.e., increase the disorder) of the prepared glass system [35]. An additional informative parameter which linked to Urbach energy is interplay of electrons with phonons parameter,E_{e-p}. It is the required energy to bind pair of the free electrons in material. The E_{e-p} could be determined from the next relation [35,48]:

$E_{e-p} = \frac{2E_u}{3K_BT}$ (6)

The resulting values of E_{e-p} were recorded in Table 3. The increment in such values with PbO content indicate that there are more free electrons in the material lattice, reflecting a fundamental decrement in the band gap.

3.6. Nonlinearity Analysis

Basically, the refractive index, *n*, is an effective parameter to study the subtle modifications in structural morphology that induced by the light propagation in the material. Refractive index could be determined by the Dimitrov and Sakka relationship [49]:

$\frac{n^2-1}{n^2+2} = 1 - \sqrt{\frac{E_g}{20}}$(7)

The obtained values of refractive index were tabulated in Table 3. It is known that the materials that have a high dense crystal structure exhibit a high refractive index. Therefore, the augmentation in the refractive index is ascribed to the high atomic weight and high polarizability of Pb^{2+} ions at the expense of the low atomic weight and low polarizability of the B^{3+}[1,28,46]. The increment in refractive index can be useful for using such material in optoelectronic applications [1,25].

Nonlinearity phenomena of materials is detected when the material's responsibility relies nonlinearly on the strength of electric field which results from the incident electromagnetic radiation. The nonlinearity investigation provides additional information about the applicability of prepared glass samples in the optical and optoelectronic devices. There are many examples of nonlinear optical interactions that lead to many applications. One of such applications is third order susceptibility, $\chi^{(3)}$, (i.e., the nonlinear optical susceptibility). Additional it is used to describe the intensity dependent refractive index.

The nonlinear optical susceptibility is, enough, related to the linear refractive index, *n*, through the next relation [50]:

$\chi^3 = \frac{A}{256\pi^4}[(n^2-1)^4]$(8)

where*n* is the linear refractive index, and A = 1.7×10^{-10} esu.

The nonlinear refractive index, n_2, is, too, related to the nonlinear optical susceptibility through the following relationship [50]:

$n_2 = \frac{12\pi}{n}\chi^3$ (9)

Where*n* is the linear refractive index. Table 3 furnishes the obtained values of both $\chi^3$and n_2. The obtained values show an incremental propensity with the increasing addendum of PbO, indicating that the doping process enhances the nonlinear characteristics of the prepared glass samples. As mentioned before, the mitigated E_g and the augmented E_u are due to the high structural impurities. Such high defects lead to the enhanced nonlinear properties [51],making the glass samples suitable for optical switching, image processing and image manipulation [52].

Sample (mol. %)	E_g (eV)	E_u (eV)	*M*	*S*	E_{e-p}	*N*	$\chi^{(3)}$ ($\times10^{-12}$)	n_{nl} ($\times10^{-11}$)
0 Pb	4.475	0.463	0.473	0.055	12.05	2.083	0.844	1.52
5 Pb	3.676	0.492	0.428	0.052	12.81	2.235	1.72	2.91
10 Pb	3.512	0.520	0.419	0.049	13.53	2.271	2.02	3.36
15 Pb	3.431	0.742	0.414	0.034	19.33	2.289	2.19	3.61
20 Pb	3.255	0.987	0.403	0.025	25.69	2.331	3.08	4.90

Table 3: Optical band gap (E_g), Urbach energy (E_u), metallization criterion (*M*), steepness coefficient (*S*), Electron-Phonon interaction (E_{e-p}), refractive index (*n*), nonlinear optical susceptibility ($\chi^{(3)}$) and nonlinear refractive index, (n_2) for all glass samples.

IV. Conclusion

In this study, five samples, with different concentrations of PbO with fixed ration of Sm_2O_3 were schemed in quaternary composition, were successfully prepared by melt-quenching technique. The amorphous nature of samples approved by XRD measurement. Density was varied from (2.40 g/cm^3)to (3.16 g/cm^3) with PbO content. This is back to the changes in the molecular weight. FTIR measurement examined the structural units and the accompanied modulations resulting from the structural changes. A Gaussian deconvolution process was utilized to compute the ratios of BO_4 and BO_3 units. Additionally, the glass transition temperature and delayed crystallization temperature were found to increase with PbO addition. The glass samples exhibit an enhanced thermal stability required for working devices. The absorption spectra of all samples exhibit sixteen absorption bands related to Sm^{3+} ions. Such transitions were carefully assigned to *4f-4f* transition of samarium ions. There are four transitions [$^6H_{5/2} \rightarrow {}^6F_{11/2}$, $^6F_{9/2}$, $^6F_{7/2}$, and $^6F_{5/2}$ corresponding to 1075,1223, 1366, and 1470 nm] have relatively higher intensities. Such intensive peaks are promising for using in optoelectronic and photonics applications. The absorption edges were found to undergo a red shift, reflecting a mitigated optical band gap changed from 4.47 eV to 3.25 eV. Additionally, increasing the disorder in samples leads to enhance the Urbach energy. Related optical parameters were precisely determined through the lead oxide addition such as mitigated metallization criterion (0.473-0.403), mitigated steepness parameters (0.055-0.025), and enhanced electron-phonon coefficient (12.05-25.69). The nonlinearity such as nonlinear optical susceptibility, linear refractive index, and non-linear refractive index were increased reflecting a high suitability to consider such samples as a decent contender for optoelectronic applications. Finally, the structure-property correlation and its conceivable interplay through PbO doping, render these hybrid glasses as a decent material for optoelectronic and optical devices realm.

Acknowledgements

This research was supported by to *Dr. Abd El Razaq Solid States Department, Faculty of Science, South Valley University* and Dr. *Hesham Yahia Amin, Basic Science Department, Faculty of Engineering Science, Sinai University,* for his consultation and assistance during this work.

References

[1]. Kavaz, E., Ghanim, E. H., &Abouhaswa, A. S. (2020). Optical, structural and nuclear radiation security properties of newly fabricated V2O5-SrO-PbO glass system. Journal of Non-Crystalline Solids, 538, 120045.
[2]. Abouhaswa, A. S., Rammah, Y. S., Ibrahim, S. E., & El-Hamalawy, A. A. (2018). Structural, optical, and electrical characterization of borate glasses doped with SnO2. Journal of Non-Crystalline Solids, 494, 59-65.
[3]. Kumar, A. S., Narendrudu, T., Suresh, S., Rao, M. S., Ram, G. C., & Rao, D. K. (2016). Role of titanium ions on the physical and structural properties of calcium zinc bismuth phosphate glass ceramics. Journal of Non-Crystalline Solids, 434, 62-70.
[4]. Mhareb, M. H. A. (2020). Physical, optical and shielding features of Li2O–B2O3–MgO–Er2O3 glasses co-doped of Sm2O3. Applied physics A, 126(1), 1-8.
[5]. Zagrai, M., Suciu, R. C., Rada, S., Pică, M. E., &Pruneanu, S. (2021). Structural and optical properties of Eu3+ ions in lead glass for photonic applications. Journal of Non-Crystalline Solids, 569, 120988.
[6]. Elkhoshkhany, N., Marzouk, S. Y., Khattab, M. A., &Dessouki, S. A. (2018). Influence of Sm2O3 addition on Judd-Ofelt parameters, thermal and optical properties of the TeO2-Li2O-ZnO-Nb2O5 glass system. Materials Characterization, 144, 274-286.
[7]. Sailaja, B., Stella, R. J., Rao, G. T., Raja, B. J., Manjari, V. P., &Ravikumar, R. V. S. S. N. (2015). Physical, structural and spectroscopic investigations of Sm3+ doped ZnO mixed alkali borate glass. Journal of Molecular Structure, 1096, 129-135.
[8]. Shaaban, K. S., El-Maaref, A. A., Abdelawwad, M., Saddeek, Y. B., Wilke, H., &Hillmer, H. (2018). Spectroscopic properties and Judd-Ofelt analysis of Dy3+ ions in molybdenum borosilicate glasses. Journal of Luminescence, 196, 477-484.
[9]. Rodrigues, R. V., Muri, E. J. B., Cruz, P. C. M., Oliveira, R. C. S., Borges, A. S., Khan, L. U.,&Stręk, W. (2020). Optical properties and Judd–Ofelt analysis of Sm3+ ions in Sm2O2S: Reddish-orange emission and thermal stability. Optical Materials, 107, 110160.
[10]. Gaikwad, D. K., Sayyed, M. I., Obaid, S. S., Issa, S. A., &Pawar, P. P. (2018). Gamma ray shielding properties of TeO2-ZnF2-As2O3-Sm2O3 glasses. Journal of Alloys and Compounds, 765, 451-458.
[11]. Mora-Ramírez, M. A., Santisteban, H. J., Portillo, M. C., Santiago, A. C., Díaz, A. R., Téllez, V. C., & Moreno, O. P. (2021). Optical emission bands of Sm2O3 and their link with crystalline defects and 4fd→ 4fd electronic transitions at UV-Vis region. Optik, 241, 167211.
[12]. Deepa, A. V., Priya, M., & Suresh, S. (2016). Influence of Samarium Oxide ions on structural and optical properties of borate glasses. Scientific Research and Essays, 11(5), 57-63.
[13]. Kilic, G., Issa, S. A., Ilik, E., Kilicoglu, O., Issever, U. G., El-Mallawany, R., ... &Tekin, H. O. (2021). Physical, thermal, optical, structural and nuclear radiation shielding properties of Sm2O3 reinforced borotellurite glasses. Ceramics International, 47(5), 6154-6168.`
[14]. Mawlud, S. Q., Ameena, M. M., Sahar, M. R., Mahraz, Z. A. S., & Ahmed, K. F. (2017, September). Thermal stability and Judd-Ofelt analysis of optical properties of Sm3+-doped sodium tellurite glasses. In AIP Conference Proceedings (Vol. 1888, No. 1, p. 020032). AIP Publishing LLC
[15]. Sreedhar, V. B., Basavapoornima, C., &Jayasankar, C. K. (2014). Spectroscopic and fluorescence properties of Sm3+-doped zincfluorophosphate glasses. Journal of Rare Earths, 32(10), 918-926.
[16]. Kindrat, I. I., Padlyak, B. V., &Drzewiecki, A. (2015). Luminescence properties of the Sm-doped borate glasses. Journal of luminescence, 166, 264-275.
[17]. El-Zaiat, S. Y., El-Den, M. B., El-Kameesy, S. U., & El-Gammam, Y. A. (2012). Spectral dispersion of linear optical properties for Sm2O3 doped B2O3–PbO–Al2O3 glasses. Optics & Laser Technology, 44(5), 1270-1276.

[18]. Laariedh, F., Sayyed, M. I., Kumar, A., Tekin, H. O., Kaur, R., &Badeche, T. B. (2019). Studies on the structural, optical and radiation shielding properties of (50–x) PbO–10 WO3–10 Na2O–10 MgO–(20+ x) B2O3 glasses. Journal of Non-Crystalline Solids, 513, 159-166.

[19]. Abdel-Wahed, M. H., Abdou, S. M., El-Bayoumi, A. S., Salem, S. M., &Bendary, A. A. (2020). Structural, optical properties and γ-ray shielding parameters of PbO embedded Li2O borophosphate glass systems. Journal of Non-Crystalline Solids, 543, 120135.

[20]. Forestier, X., Cimek, J., Kujawa, I., Kasztelanic, R., Pysz, D., Orliński, K., ... &Buczyński, R. (2019). Study of SiO2-PbO-CdO-Ga2O3 glass system for mid-infrared optical elements. Journal of non-crystalline solids, 503, 52-61.

[21]. Smolík, J., Knotek, P., Schwarz, J., Černošková, E., Kutálek, P., Kralova, V., &Tichý, L. (2021). Laser direct writing into PbO-Ga2O3 glassy system: Parameters influencing microlenses formation. Applied Surface Science, 540, 148368.

[22]. Singh, G. P., Singh, J., Kaur, P., Kaur, S., Arora, D., Kaur, R., ... & Singh, D. P. (2020). Analysis of enhancement in gamma ray shielding proficiency by adding WO3 in Al2O3-PbO-B2O3 glasses using Phy-X/PSD. Journal of Materials Research and Technology, 9(6), 14425-14442.

[23]. Alotaibi, B. M., Sayyed, M. I., Kumar, A., Alotiby, M., Sharma, A., Al-Yousef, H. A., ... & Al-Hadeethi, Y. (2021). Optical and gamma-ray shielding effectiveness of a newly fabricated P2O5–CaO–Na2O–K2O–PbO glass system. Progress in Nuclear Energy, 138, 103798.

[24]. Rao, T. R., Reddy, C. V., Krishna, C. R., Thampy, U. U., Raju, R. R., Rao, P. S., &Ravikumar, R. V. S. S. N. (2011). Correlation between physical and structural properties of Co2+ doped mixed alkali zinc borate glasses. Journal of non-crystalline solids, 357(18), 3373-3380.

[25]. Hivrekar, M. M., Sable, D. B., Solunke, M. B., &Jadhav, K. M. (2018). Different property studies with network improvement of CdO doped alkali borate glass. Journal of Non-Crystalline Solids, 491, 14-23.

[26]. Rao, K. V., Babu, S., Venkataiah, G., &Ratnakaram, Y. C. (2015). Optical spectroscopy of Dy3+ doped borate glasses for luminescence applications. Journal of Molecular Structure, 1094, 274-280.

[27]. Morshidy, H. Y., Abd El-Fattah, Z. M., Abul-Magd, A. A., Hassan, M. A., & Mohamed, A. R. (2021). Reevaluation of Cr6+ optical transitions through Gd2O3 doping of chromium-borate glasses. Optical Materials, 113, 110881.

[28]. Abul-Magd, A. A., Morshidy, H. Y., & Abdel-Ghany, A. M. (2020). The role of NiO on the structural and optical properties of sodium zinc borate glasses. Optical Materials, 109, 110301.

[29]. Shannon, R. D. (1976). Revised effective ionic radii and systematic studies of interatomic distances in halides and chalcogenides. Actacrystallographica section A: crystal physics, diffraction, theoretical and general crystallography, 32(5), 751-767.

[30]. H.Y. Morshidy, A.R. Mohamed, A.A. Abul-magd, M.A. Hassan, Role of high energy Cr 6 + optical transition induced by rare earth ion (La 3 +) in compositional-dependent borate glass, Mater. Chem. Phys. 289 (2022) 126503. https://doi.org/10.1016/j.matchemphys.2022.126503.

[31]. Hassan, M. A. (2013). Effect of halides addition on the ligand field of chromium in alkali borate glasses. Journal of alloys and compounds, 574, 391-397.

[32]. Salama, E., Maher, A., & Youssef, G. M. (2019). Gamma radiation and neutron shielding properties of transparent alkali borosilicate glass containing lead. Journal of Physics and Chemistry of Solids, 131, 139-147.

[33]. Morshidy, H. Y., Sadeq, M. S., Mohamed, A. R., & El-Okr, M. M. (2020). The role of CuCl2 in tuning the physical, structural and optical properties of some Al2O3–B2O3 glasses. Journal of Non-Crystalline Solids, 528, 119749.

[34]. Hassan, M. A., Ebrahim, F. M., Moustafa, M. G., Abd El-Fattah, Z. M., & El-Okr, M. M. (2019). Unraveling the hidden Urbach edge and Cr6+ optical transitions in borate glasses. Journal of Non-Crystalline Solids, 515, 157-164.

[35]. Morshidy, H. Y., Mohamed, A. R., Abul-Magd, A. A., & Hassan, M. A. (2022). Ascendancy of Cr3+ on Cr6+ valence state and its effect on borate glass environment through CdO doping. Materials Chemistry and Physics, 285, 126128.

[36]. Abdullah, M., Shafieza, S. N. E., Kasim, A., &Hashim, A. (2016). The effect of PbO on the physical and structural properties of borate glass system. In Materials Science Forum (Vol. 846, pp. 177-182). Trans Tech Publications Ltd.

[37]. Sreenivasulu, V., Upender, G., Mouli, V. C., & Prasad, M. (2015). Structural, thermal and optical properties of TeO2–ZnO–CdO–BaO glasses doped with VO2+. SpectrochimicaActa Part A: Molecular and Biomolecular Spectroscopy, 148, 215-222.

[38]. Kumar, A., Deopa, N., Kumar, A., Chahal, R. P., Dahiya, S., Punia, R., & Rao, A. S. (2022). Structural, thermal, optical and luminescence properties of Dy3+ ions doped Zinc Potassium Alumino Borate glasses for optoelectronics applications. Journal of Non-Crystalline Solids, 588, 121613.

[39]. Kumar, A., Kumar, V., Sahu, M. K., Dahiya, S., Deopa, N., Punia, R., & Rao, A. S. (2021). Physical, structural and optical characterization of Dy3+ doped ZnF2-WO2-B2O3-TeO2 glasses for opto-communication applications. Optical Materials, 114, 110937.

[40]. Sayyed, M. I., Almuqrin, A. H., Kumar, A., Jecong, J. F. M., &Akkurt, I. (2021). Optical, mechanical properties of TeO2-CdO-PbO-B2O3 glass systems and radiation shielding investigation using EPICS2017 library. Optik, 242, 167342.

[41]. Chen, Q., Su, K., Li, Y., & Zhao, Z. (2018). Structure, spectra and thermal, mechanical, Faraday rotation properties of novel diamagnetic SeO2-PbO-Bi2O3-B2O3 glasses. Optical Materials, 80, 216-224.

[42]. Sadeq, M. S., & Morshidy, H. Y. (2020). Effect of samarium oxide on structural, optical and electrical properties of some alumino-borate glasses with constant copper chloride. Journal of Rare Earths, 38(7), 770-775.

[43]. Hemalatha, S., Nagaraja, M., Madhu, A., Suresh, K., &Srinatha, N. (2021). The role of Sm2O3 on the structural, optical and spectroscopic properties of multi-component ternary borate glasses for orange-red emission applications. Journal of Non-Crystalline Solids, 554, 120602.

[44]. Zaman, F., Srisittipokakun, N., Rooh, G., Kaewkhao, J., Ullah, I., Rani, M., & Kim, H. J. (2021). Development of Na2O-MO-Bi2O3-B2O3-Sm2O3 glasses (MO= Ba/Mg) for laser and scintillation application. Journal of Non-Crystalline Solids, 561, 120722.

[45]. Davis, E. A., & Mott, N. (1970). Conduction in non-crystalline systems V. Conductivity, optical absorption and photoconductivity in amorphous semiconductors. Philosophical magazine, 22(179), 0903-0922.

[46]. Saddeek, Y. B., Aly, K. A., &Bashier, S. A. (2010). Optical study of lead borosilicate glasses. Physica B: Condensed Matter, 405(10), 2407-2412.

[47]. [47] Urbach, F. (1953). The long-wavelength edge of photographic sensitivity and of the electronic absorption of solids. Physical Review, 92(5), 1324.

[48]. Rice, T. M. (2011). The future of superconductivity viewed through a cloudy crystal ball. In Contemporary Concepts of Condensed Matter Science (Vol. 4, pp. 235-251). Elsevier.

[49]. Dimitrov, V., & Sakka, S. (1996). Linear and nonlinear optical properties of simple oxides. II. Journal of applied physics, 79(3), 1741-1745.

[50]. Ticha, H., &Tichy, L. (2002). Semiempirical relation between non-linear susceptibility (refractive index), linear refractive index and optical gap and its application to amorphous chalcogenides. J. Optoelectron. Adv. Mater, 4(2), 381-386.
[51]. Sayyed, M. I., Ibrahim, A., Abdo, M. A., &Sadeq, M. S. (2022). The combination of high optical transparency and radiation shielding effectiveness of zinc sodium borate glasses by tungsten oxide additions. Journal of Alloys and Compounds, 904, 164037.
[52]. Abuelwafa, A. A., El-Denglawey, A., Dongol, M., El-Nahass, M. M., & Soga, T. (2015). Influence of annealing temperature on structural and optical properties of nanocrystalline Platinum octaethylporphyrin (PtOEP) thin films. Optical Materials, 49, 271-278.

Heba M.Ali, et. al. "Structure-Property Correlation in Lead Borate Glass with Fixed Ratio of Samarium Oxide." *IOSR Journal of Applied Physics (IOSR-JAP)*, 14(5), 2022, pp. 52-65.